Supporting Information

for

Laser Post-Ionisation Combined with a High Resolving Power Orbitrap Mass Spectrometer for Enhanced MALDI-MS Imaging of Lipids

S. R. Ellis,*[a], J. Soltwisch[b, c], M. R. L. Paine[a] , K. Dreisewerd[b, c] and R. M. A. Heeren[a]

[a] M4I, The Maastricht Multimodal Molecular Imaging Institute, University of Maastricht, 6229 ER Maastricht, The Netherlands

[b]Institute for Hygiene, University of Münster, Robert-Koch-Strasse 41, 48149 Münster, Germany

[c] Interdisciplinary Center for Clinical Research (IZKF), University of Münster, Domagkstrasse 3, 48149 Münster, Germany

Table of Contents

Experimental Methods

Materials

Methanol (MeOH), ethanol (EtOH), and xylene were purchased from Biosolve (Valkenswaard, The Netherlands). Chloroform ($CHCl_3$, anhydrous, ≥99%), and norharmane (9H-pyrido[3,4-b]indole) matrix, hematoxylin (H) solution modified according to Gill II, and eosin (E) solution (0.5% ethanol) were purchased from Sigma Aldrich (Zwijndrecht, The Netherlands). Indium tin oxide (ITO) coated glass slides (4–8 Ω/sq) were purchased from Delta Electronics (Loveland, CO, USA).

Tissue Preparation

For imaging experiments, fresh frozen rat brain sections of 10 µm thickness were prepared using a cryomicrotome (Microm International, Walldorf, Germany) and mounted onto ITO-coated glass slides. Prior to matrix application tissues were dried under a gentle stream of nitrogen for 30 s. For positive and negative ion lipid imaging a norharmane matrix solution (7 mg/mL 7:3 $CHCl_3$:MeOH (v/v)) was applied to the tissues using a TM-Sprayer (HTX Technologies, Chapel Hill, NC, USA). The matrix solution was applied using a flow rate of 0.12 mL/min and an N_2 pressure of 10 psi and a gas temperature of 30 °C. The pneumatic spray traversed the area of the sample at a velocity of 1200 mm/min with 3 mm track spacing. Ten layers of matrix were applied to the surface under these conditions, with 30 s drying time between each layer. To compare the effects of washing the tissue prior to analysis (data not shown), tissues were submerged in a cooled aqueous solution of ammonium formate (100 mM, 4 °C) for a period of 15 s, dried under a flow of nitrogen, and then submerged again in a

fresh batch of cooled ammonium formate solution for 15 s. This tissue was used to generate the data shown in Fig. 1.

Tissue Staining

After tissues were analysed by MSI the remaining matrix was washed from the tissue by gently shaking it in a Petri dish in 95% EtOH for 20 s. A standard H&E protocol was used for staining afterwards (95% EtOH, 70% EtOH, H_2O for 30 s each, hematoxylin for 3 minutes, H_2O, 70% EtOH, 95% EtOH for 30 s, eosin for 1 min, 95% and 100% EtOH for 30 s each, xylene for 2 min). The sections were covered with cover slips using Cytoseal XYL (Richard-Allan Scientific, Kalamazoo, MI, USA) and allowed to dry. The stained preparations were scanned using a Nikon Super COOLSCAN 5000 ED film scanner (Nikon, Melville, NY, USA).

Mass Spectrometry Imaging (MSI) Instrumentation

All experiments were performed with an Orbitrap Elite mass spectrometer (Thermo Fisher Scientific, Bremen, Germany). To enable MALDI-MSI the system was coupled to an intermediate pressure MALDI source based on a dual ion funnel interface (Spectroglyph LLC, Kennewick, WA, USA) that replaced the standard S-lens assembly of the Orbitrap.

For all MSI experiments the high pressure ion funnel was operated at pressure 5.3 mbar (positive ion mode) and 6.7 mbar (negative ion mode) while the low pressure funnel was always maintained at 2 mbar. Both the high and low pressure funnels were operated at an amplitude of ~80 $V_{0\text{-}p}$ and a frequency of 710 kHz and 990 kHz, respectively.. Ions were

extracted from the sample into the funnel entrance via a potential difference of 80 V between the sample holder and the first electrode of the funnel.

A schematic of the optical setup is provided in Fig. S1. MALDI ion production was initiated via an actively Q-switched frequency-tripled Nd:YLF laser (Explorer One, Spectra Physics, Mountain View, CA, USA) emitting 5 ns long pulses of 349 nm wavelength at a pulse repetition rate of 100 Hz. Unless for the experiments used to record Fig. 1 a pulse energy of ~1.4 µJ was used, a factor of about 3 above the ion detection threshold of ~500 nJ. Pulse energies were measured using the internal photodiode provided with the Explorer laser. The MALDI laser beam was guided onto the sample via 2 UV-grade aluminium mirrors (Thorlabs, Newton, NJ, USA) where it then passes through a 20x beam expander (Wavelength Opto-Electronics, Singapore) and a 200 mm focal length plano-convex lens for final focussing. After propagation through the lens the light is reflected by a dielectrically coated mirror. Fine adjustment of this mirror enabled final steering of the beam onto the sample. Using this set-up an effective focal spot size of 15-20 µm in diameter was obtained, as measured by the ablation patterns produced in a homogenous norharmane matrix layer.

For post-ionisation a wavelength tunable optical parametric oscillator laser system (NT-230, Ekspla, Vilnius, Lithuania) was used. This system incorporates a Q-switched frequency-tripled Nd:YAG laser as pump source. The width of the OPO emission pulse is about 5 ns. For all experiments presented the OPO laser was tuned to 280 nm and a pulse energy of ~800 µJ after attenuation (unattenuated the output was ~1.6 mJ for 280 nm). For the reported MALDI-2-MSI experiments the pulse repetition rate was set to the maximum possible of 100 Hz. To couple the PI laser beam to the ion funnel source, the OPO beam was steered via a UV-grade fused silica mirror (1-OS-2-0127-5-[1A45-GDD], Altechna, Vilnius, Lithuania) providing a peak reflectivity at 260 nm. A Glan-Taylor polariser (α-BBO, 2-GT-2235-2, Altechna, Vilnius, Lithuania) was used for adjustable energy attenuation. The beam is

reflected again by another identical mirror onto a UV-fused silica right angled prism (PR-1254-220-330, Altechna, Vilnius, Lithuania). Using the prism the beam is steered through a 25.4 mm diameter UF-fused silica lens (f = 400 mm, PCX-2-L254, Altechna, Vilnius, Lithuania) and finally through a ½ inch UV-fused silica window installed on the side of the MALDI source housing. The beam path inside the ion source was established to be parallel to the sample plate and to intersect the MALDI plume ~400 µm above the sample surface and exhibiting a focal taille of ~200 µm by diameter as determined by burn patterns in mounted paper. To register the output pulse of the OPO laser a photodiode detector (DET-10A, Thor Labs, Germany) was placed behind the second mirror of the OPO beam path where it collected partially transmitted light. The Explorer 349 nm MALDI laser provides an output signal recorded with an internal photodiode that can readily be used for synchronisation. Both photodiode outputs were monitored with a fast digital oscilloscope. To precisely control the timing (*i.e.*, the delay between the laser pulses) both lasers were externally triggered using a precision delay generator (DG-645 Stanford Research Systems, Sunnyvale, CA, USA). The pulse generator was internally triggered at 100 Hz and time-displaced trigger signals sent to each laser. The timing of the pulses was then easily adjustable by controlling the delay between the internal trigger pulse and the external trigger sent to each laser. For all experiments presented here the delay between the MALDI and post-ionisation laser pulses was 18 µs.

MSI Data Acquisitions

All MSI data was acquired using the maximum 240,000 FWHM (at *m/*z 400) mass resolution setting and a 250 ms injection time. This resulted in a scan time of 1.06 sec/scan. The "automatic gain control" was turned off. MALDI sample stage motion was synchronised with the beginning of the injection event. At 100 Hz this means that ~25 laser shots are collected to probe each pixel during MSI experiments. MSI data were acquired across an *m/z* range of 350-2000. Mass accuracy of MSI data was typically better than 2 ppm. To enable direct comparison between MALDI and MALDI-2 both datasets were acquired sequentially on the same tissue section. First, the MALDI-2 dataset was acquired with a pitch width (step size of sample stage movement) of 100 µm×100 µm. After completing the MALDI-2-MSI run, the image was reacquired with conventional MALDI using a newly drawn measurement region over the same area. Given a focal laser spot size of ~20 µm in diameter the probability of analysing the same positions was low but not negligible. After both datasets were collected optical microscopy of the analysed tissues was therefore performed to confirm the sampling positions did not overlap for any of the presented MSI data. As a result, both datasets were thus acquired from the same tissue without interfering each other, yet enabling direct comparison of mass spectra. Due to the relatively high source pressure maintained in the ion funnel source no sizable evaporation of norharmane matrix (i.e., loss of matrix or analyte ion signals) was observed over hours of MSI operation.

Tandem Mass Spectrometry

Tandem mass spectrometry was performed directly on tissue using collision-induced dissociation (CID) and typically with ion trap detection due to its higher intrinsic sensitivity. Normalised collision energies were 30% and 40% for positive and negative ion mode

measurements respectively. In cases where detection of low *m/z* fragments, accurate mass and differential assignment of isobaric ions was required (*i.e.,* to confirm assignments made for Fig. 3 (Fig. S8) and Fig. 5 (Fig. S18) and for characterisation of matrix adducts (Fig. S9 and S10) fragments were generated with higher energy collision-induced dissociation (HCD) and product ions detected with the Orbitrap (240,000 FWHM resolution setting). Due to the partially low abundance of the precursor ions in analysed in Figs S8 and S10 a 5000 ms injection time was used while the stage was continuously moved across the sample manually. In all cases an isolation window of 1 *m/*z unit was employed.

Data Visualisation

MSI data was reconstructed and visualised using in-house developed software written in MATLAB (MATLAB (Matlab; Mathworks, Natick, MA, USA; R2013a). Thermo Fisher .raw data as provided by the Xcalibur instrument software were first converted to .mzxml format using the MassMatrix File Conversion Tools 3.9. For image visualisation data was binned in 1.5 mDa intervals and peak-picked using the PEAPI algorithm.[1] Average spectra from each dataset were generated following a similar approach to Xcalibur data analysis software using Peak-by-Peak framework (Spectroswiss, Lausanne, Switzerland). Importantly, Peak-by-Peak enables quick, 1-5 minutes per dataset, data processing of the large imaging FTMS datasets (full profile mass spectra in .raw file format). All images are presented without any normalisation applied.

Lipid Nomenclature

Lipid nomenclature is based on the recommendations of the Lipid MAPS consortium and those discussed in Liebisch *et al.*[2, 3] Glycerophospholipid and sphingolipid classes are indicated by a two letter abbreviation. For example, PE corresponds to a phosphatidylethanolamine and GalCer corresponds to a galactosylceramde. Individual fatty acyls are indicated in the format of "total number of carbons:number of double bonds". For example 18:1 indicates a fatty acyl containing 18 carbons and one double bond. In case of lipids containing two fatty acyls each is separated by an underscore. The underscore indicates the *sn*-position of the fatty acyls is unknown. For example PE(18:1_22:6) indicates a phosphatidylethanolamine containing an 18:1 and a 22:6 fatty acid with unknown *sn* positions. In cases where assignment of individual fatty acyls was not possible the sum composition of both fatty acids is indicated. For example PE(40:7) indicates a phosphatidylethanolamine contain 40 carbons and 7 double bonds spread across both fatty acyl moieties. For ether bound fatty acyls these are preceded with either an "O" or a "P" indicating a 1-*O*-alkyl ether and a 1-*O*-alkenyl ether (plasmalogen), respectively. Note the number of indicated fatty acyl double bonds excludes those arising from 1-O-alkenyl moieties. In cases where these cannot be distinguished both possibilities are provided. We note given the limitations of CID and HCD it is often not possible to assign *sn* or double bond positions and many reported lipids likely exists as a mixture of structural isomers.

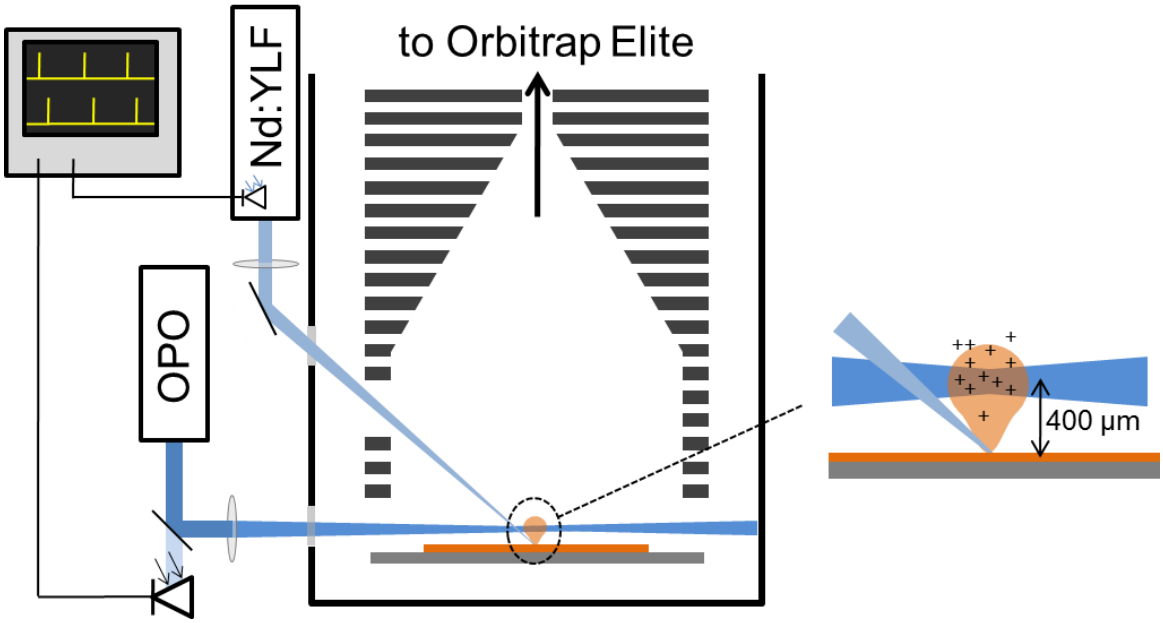

Fig S1. Schematic of the experimental set-up showing the coupling of the MALDI and OPO post-ionization laser beams to the dual funnel MALDI ion source.

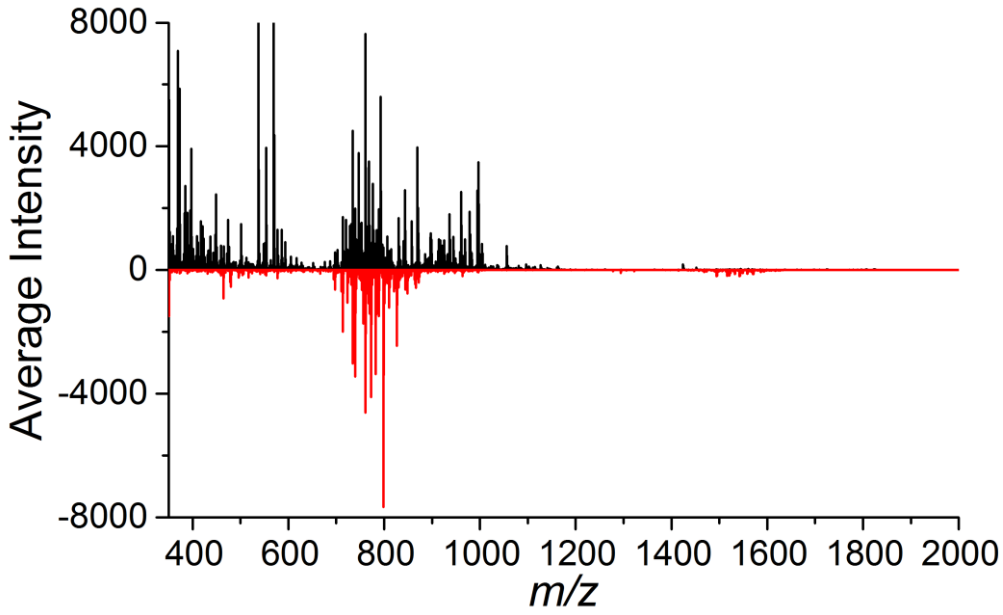

Fig. S2. Full average positive ion mode MALDI-2 (top) and conventional MALDI (bottom) mass spectra acquired from a rat brain tissue section and showing the *m/z* 350-2000 range. The same data set as for Fig. 2a of the main text was evaluated.

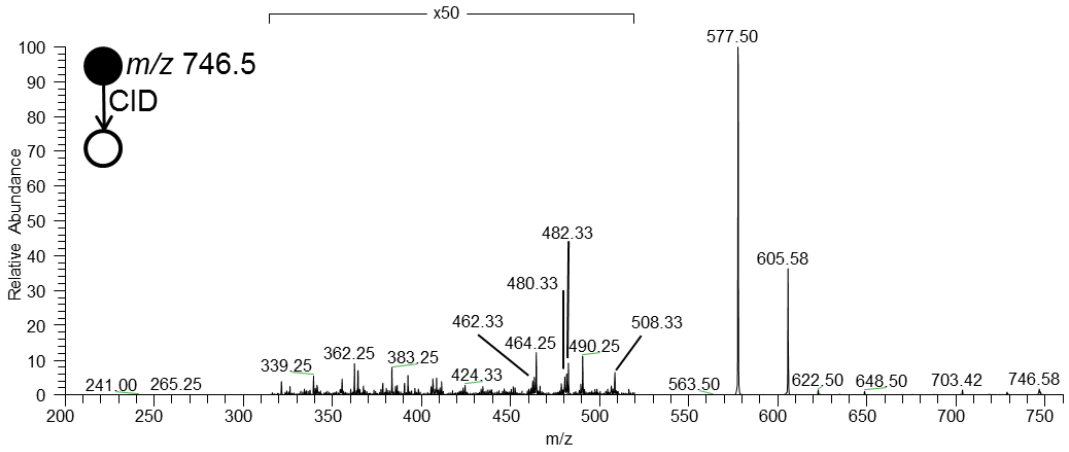

Fig. S3. Low-energy CID MS/MS spectrum of the ions at *m/z* 746.5 detected from rat brain tissue in positive ion mode using the linear ion trap. A fragment supporting the assignment of $[PE(36:1)+H]^+$ is found at *m/z* 605 (loss of phosphoethanolamine). Tentatively, this lipid is assigned to $[PE(18:0\_18:1)+H]^+$ based on the presence of fragments at *m/z* 464 and 482 (loss of 18:1 as fatty acid and ketene) and a low abundance fragment at *m/z* 462 (loss of 18:0 fatty acid). Fragments supporting the assignment of DMPE (16:0_18:1) are found at *m/z* 577 (loss of N, N-dimethylethenamine), *m/z* 464 and 482 (loss of 18:1 as fatty acid and ketene) and *m/z* 490 and 508 (loss of 16:0 as fatty acid and ketene). Due to the isolation width of 1 *m/z* unit additional isobaric and isomeric lipids are potentially also fragmented giving rise to additional product ions.

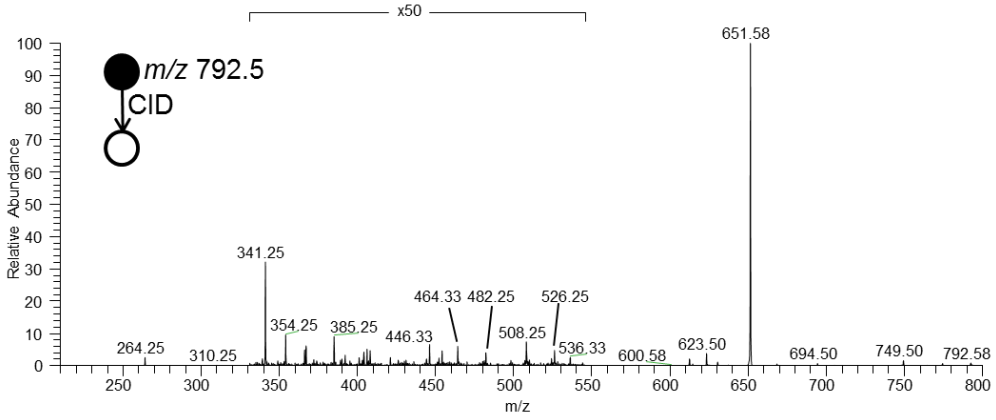

Fig. S4. Low-energy CID MS/MS spectrum of the ions at *m/z* 792.5 detected from rat brain tissue in positive ion mode using the linear ion trap. Fragment ions supporting the assignment of $[PE(18:0\_22:6)+H]^+$ are found at *m/z* 651 (loss of phosphoethanolamine), *m/z* 464 and 482 (loss of 22:6 as fatty acid and ketene) and *m/z* 508 and 526 (loss of 18:0 as fatty acid and ketene). Due to the isolation width of 1 *m/z* unit additional isobaric and isomeric lipids are potentially also fragmented giving rise to additional product ions.

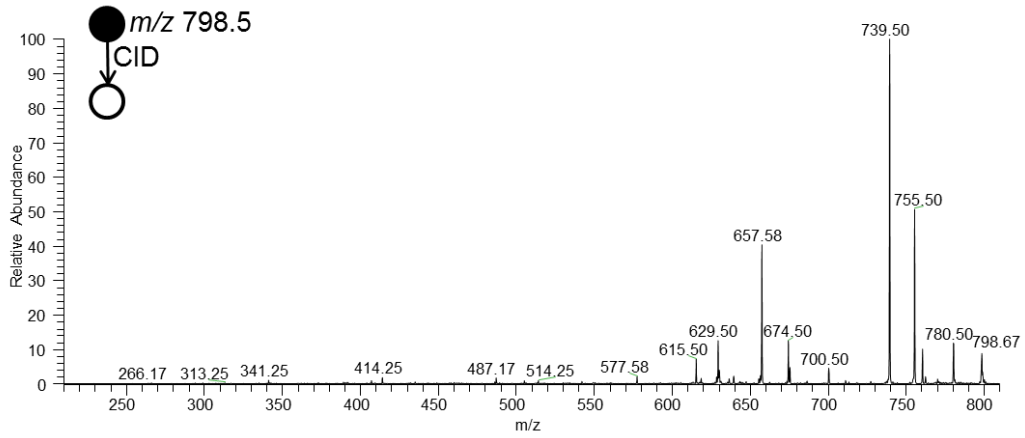

Fig. S5. Low energy CID MS/MS CID spectrum of the ions at *m/z* 798.5 detected from rat brain tissue in positive ion mode using the linear ion trap. Fragments supporting the assignment of $[PC(34:1)+K]^+$ are found at *m/z* 739 (loss of trimethyalamine), *m/z* 615 (loss of cyclophosphane from *m/z* 739) and *m/z* 577 (loss of potassiated cyclophosphane from *m/z* 739). Due to the isolation width of 1 *m/z* unit additional isobaric and isomeric lipids are also fragmented giving rise to additional fragment ions.

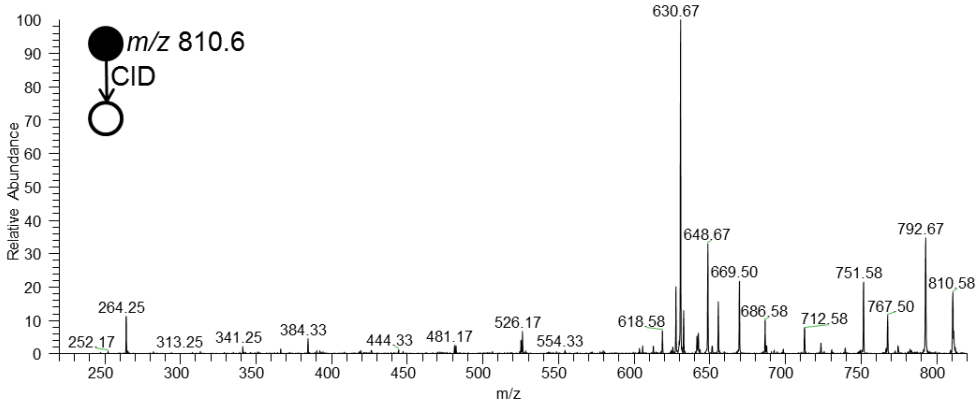

Fig. S6. Low-energy CID MS/MS spectrum of the ions at *m/z* 810.6 detected from rat brain tissue in positive ion mode using the linear ion trap. Fragment ions supporting the assignment of $[GalCer(d18:1/24:1)+H]^+$ are found at *m/z* 630 and 648 (loss of galactose and galactose-H_2O) and at *m/z* 264 ($[sphingosine\text{-}2H_2O+H]^+$). Due to the isolation width of 1 *m/z* unit additional isobaric and isomeric lipids are also fragmented giving rise to additional fragment ions. Note the sugar unit is assumed to be galactose.

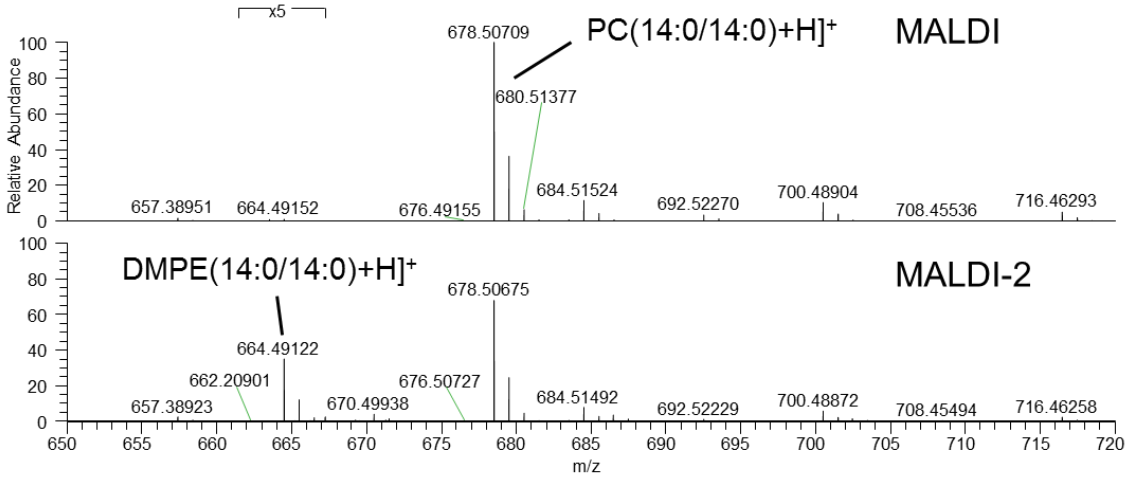

Fig. S7. Average MALDI (top) and MALDI-2 (bottom) Orbitrap mass spectra acquired from a PC (14:0/14:0) standard mixed with norharmane matrix solution and deposited onto an ITO slide. In the case of MALDI-2 a significant increase in the $[M+H-CH_3]^+$ ion abundance (i.e., $[DMPE\ (14:0/14:0)+H]^+$ at *m/z* 664.49 is observed. This observations support the idea that the majority of the DMPE signal arises from PC fragmentation.

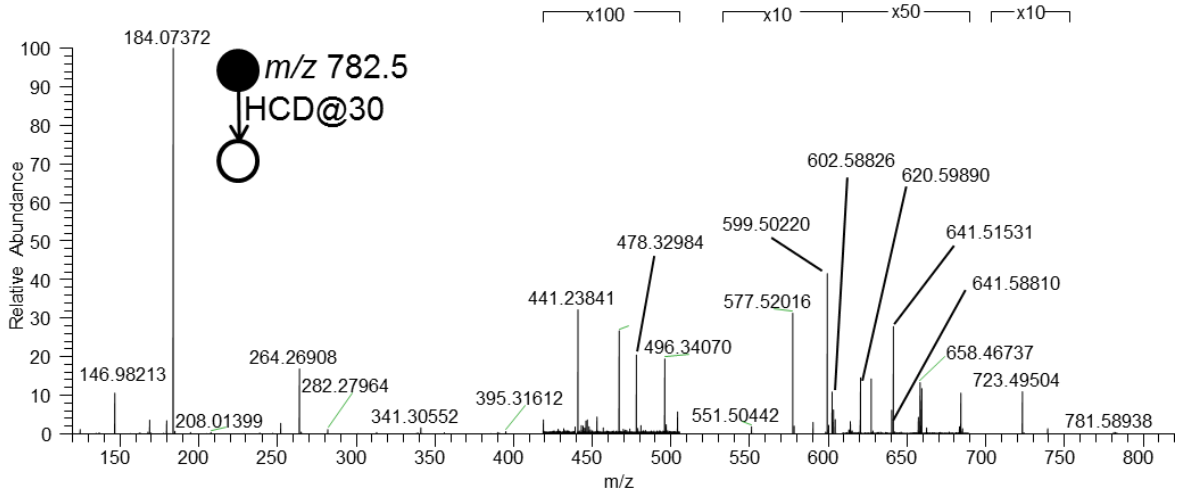

Fig. S8. Higher-energy collisional dissociation (HCD) MS/MS spectrum of the series of isobaric ions described in Fig. 3 (positive ion mode) and detected with the Orbitrap (mass resolution setting 240,000 FWHM). The peak at *m/z* 782.5 was fragmented using a normalised collision energy of 30. Fragment ions supporting the assignment of $[PC(34:1)+Na]^+$ are found at *m/z* 723.49504 (loss of trimethyalamine, 2.1 ppm), *m/z* 599.50220 (loss of cyclophosphane from the ion at *m/z* 723.49504, 2.0 ppm), *m/z* 577.52016 (loss of sodiated cyclophosphane from *m/z* 723.49504, 1.9 ppm) and *m/z* 146.98213 ($[cyclophosphane+Na]^+$, 2.5 ppm). Fragments supporting the assignment of $[PC(36:4)+H]^+$ are found at *m/z* 478.32984 and 496.34070 (loss of 20:4 as fatty acid, 1.3 ppm, and ketene, 1.9 ppm). Fragment ions supporting the assignment of $[PE(P\text{-}40:3)+H]^+/PE[O\text{-}40:4)+H]^+$ are found at *m/z* 641.58810 (loss of phosphoethanolamine, 2.1 ppm). Fragments supporting the assignment of $[GalCer(d18:1/22:1)+H]^+$ are found at *m/z* 602.58826 and 620.59890 (loss of galactose, 2.0 ppm and $[galactose\text{-}H_2O]$, 2.1 pm, respectively) and *m/z* 264.26908 ($[sphingosine\text{-}2H_2O+H]^+$, 1.9 ppm). Note that the sugar moiety is assumed to be galactose. The fragment ion at *m/z* 184.07372 corresponding to phosphocholine can arise from both $[PC(34:1)+Na]^+$ and $[PC(36:4)+H]^+$. Although not observed in this spectrum the corresponding CID/Orbitrap spectrum gives a higher relative yield of the phosphoethanolamine neutral losses and also reveals a fragment with *m/z* 641.57861 which is assigned to the neutral loss of phosphoethanolamine from $[PE(P\text{-}40:4)^{13}C_2+H]^+/[PE(O\text{-}40:5)^{13}C_2+H]^+$ (1.3 ppm). Due to the isolation width of 1 *m/z* unit additional isobaric and isomeric lipids are also fragmented giving rise to additional fragment ions.

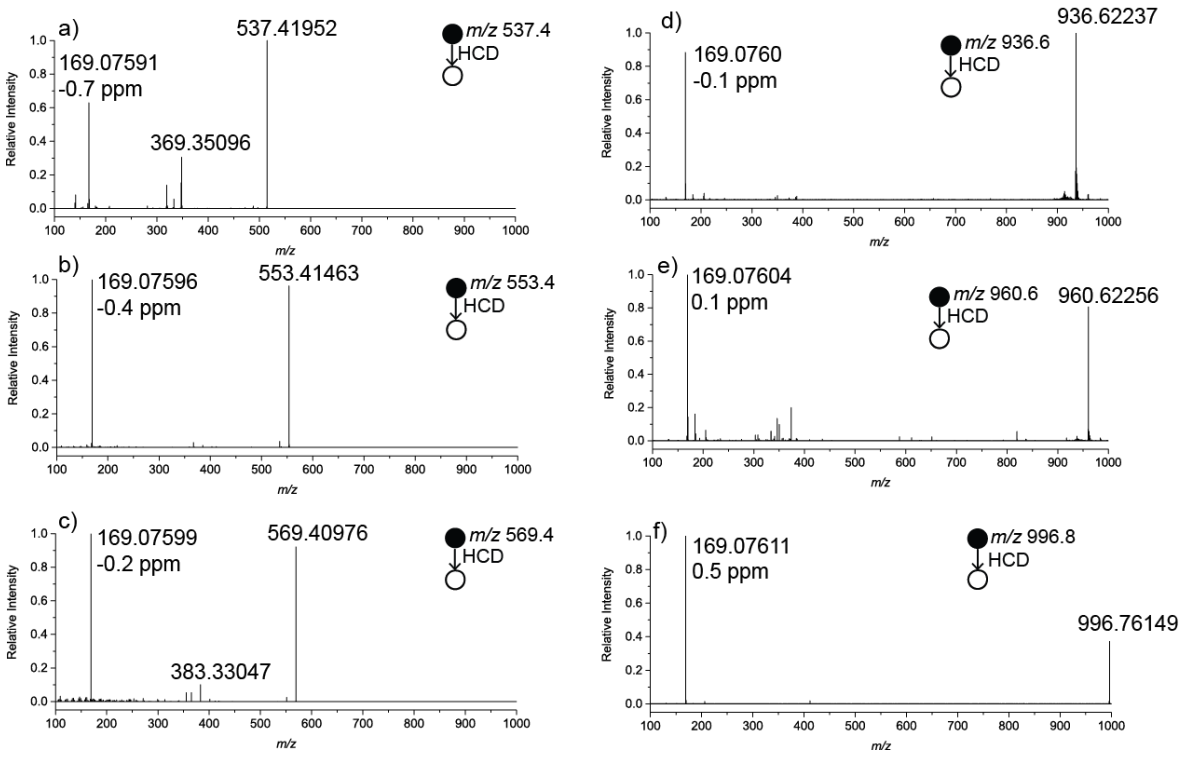

Fig. S9. Positive ion higher-energy collisional dissociation (HCD) MS/MS spectra acquired from precursor *m/z* values of (a) 537.4, (b) 553.4, (c) 569.4, (d) 936.6, (e) 960.6 and (f) 996.8 detected with the Orbitrap (mass resolution setting 240,000 FWHM). The fragment ion at *m/z* 169.07 is assigned to the $[M+H]^+$ ion of norharmane ($[C_{11}H_9N_2]^+$) and confirms the assignment of these precursors as matrix-related adducts.

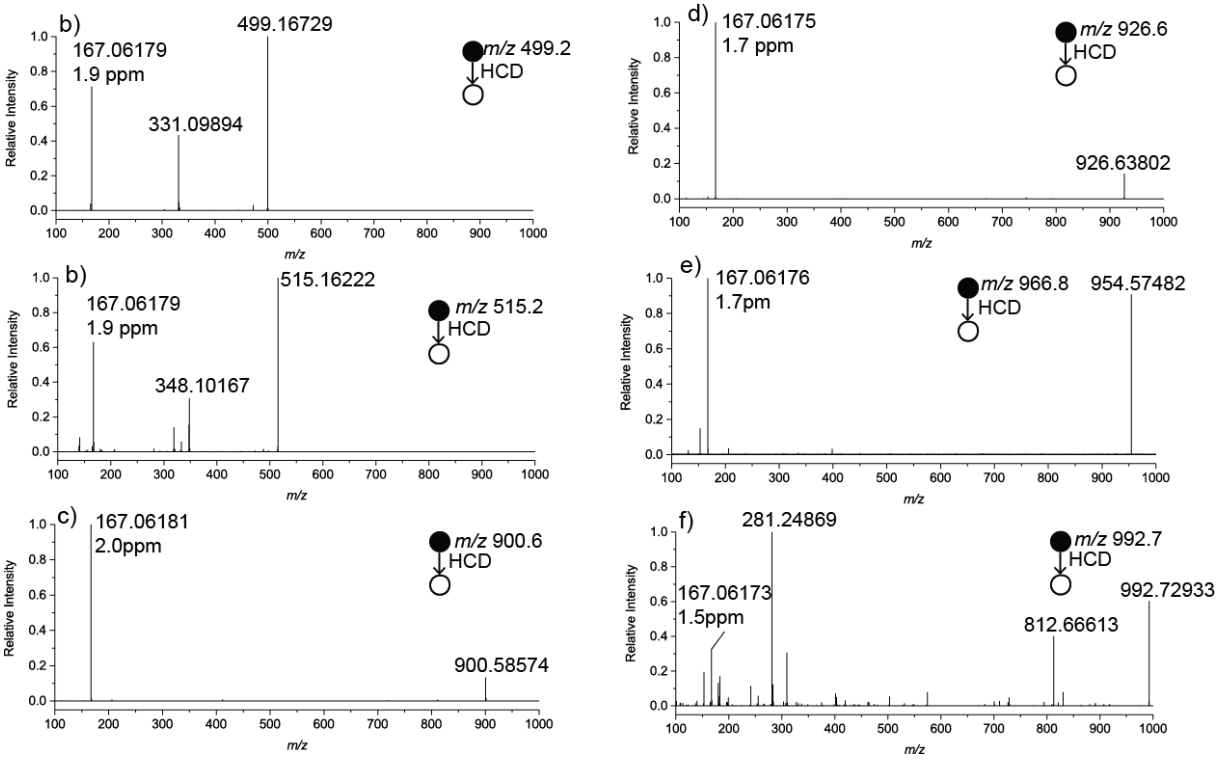

Fig. S10. Negative ion higher-energy collisional dissociation (HCD) MS/MS spectra acquired from precursor *m/z* values of (a) 499.2, (b) 515.2 (c) 900.6, (d) 926.6, (e) 954.6 and (f) 992.7 product ions were detected with the Orbitrap (mass resolution setting 240,000 FWHM). The fragment ion at *m/z* 167.07 is assigned to the $[M-H]^-$ ion of norharmane ($[C_{11}H_7N_2]^-$) and confirms the assignment of these precursors as matrix-related adducts.

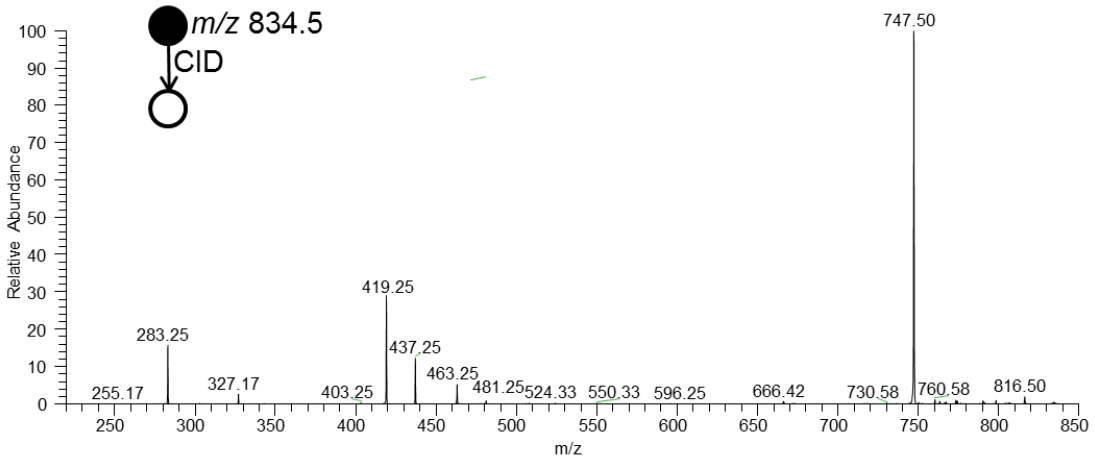

Fig. S11. Low-energy CID MS/MS spectrum of the ions at *m/z* 834.5 detected from rat brain tissue in negative ion mode using the linear ion trap. Fragment ions supporting the assignment of [PS(18:0_22:6)-H]$^-$ are found at *m/z* 747 (loss of [serine-H_2O]), *m/z* 419 and 437 (loss of 22:6 fatty acid and ketene from *m/z* 747.5), *m/z* 463 and 481 (loss of 18:0 as fatty acid and ketene from *m/z* 747.5), *m/z* 283 (18:0 fatty acid) and *m/z* 327 (22:6 fatty acid). Due to the isolation width of 1 *m/z* unit additional isobaric and isomeric lipids are also fragmented giving rise to additional fragment ions.

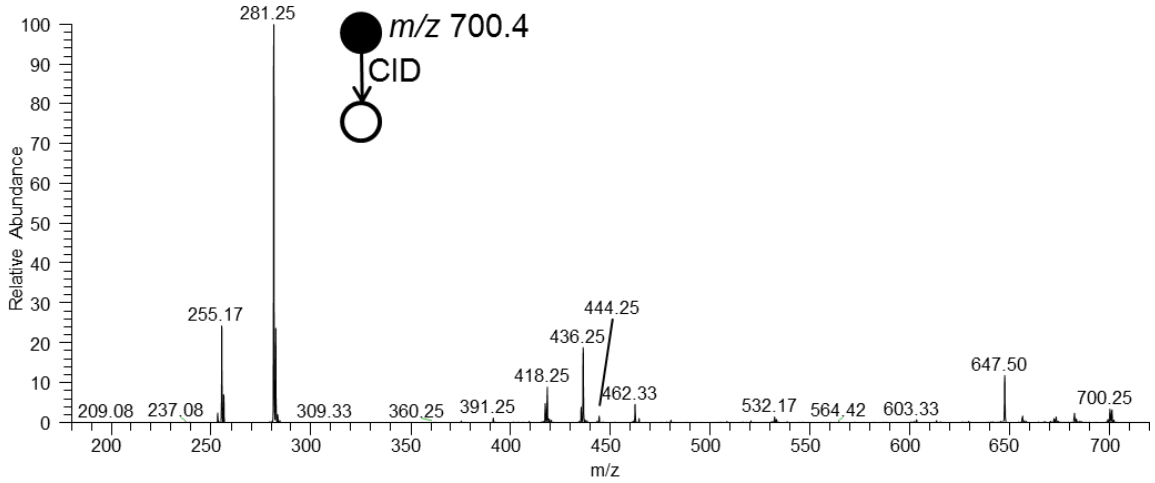

Fig. S12. Low-energy CID MS/MS spectrum of the ions at *m/z* 700.5 detected from rat brain tissue in negative ion mode using the linear ion trap. Fragments supporting the assignment of [PE(P-34:1)-H]$^-$are found at *m/z* 418 and 436 (loss of 18:1 as fatty acid and ketene), *m/z* 444 and 462 (loss of 16:0 as fatty acid and ketene), *m/z* 281 (18:1 fatty acid) and *m/z* 255 (16:0 fatty acid). The presence of these ions could indicate a mixture of isomeric [PE(P-16:0_18:1)-H]$^-$ and [PE(P-18:1_16:0)-H]$^-$. Alternatively, only one isomer may be present and the mixture of 16:0 and 18:1-related ions could arise via simultaneous isolation and fragmentation of the first ^{13}C isotope of [PA(36:2)-H]$^-$. Due to the isolation width of 1 *m/z* unit additional isobaric and isomeric lipids are also fragmented giving rise to additional fragment ions.

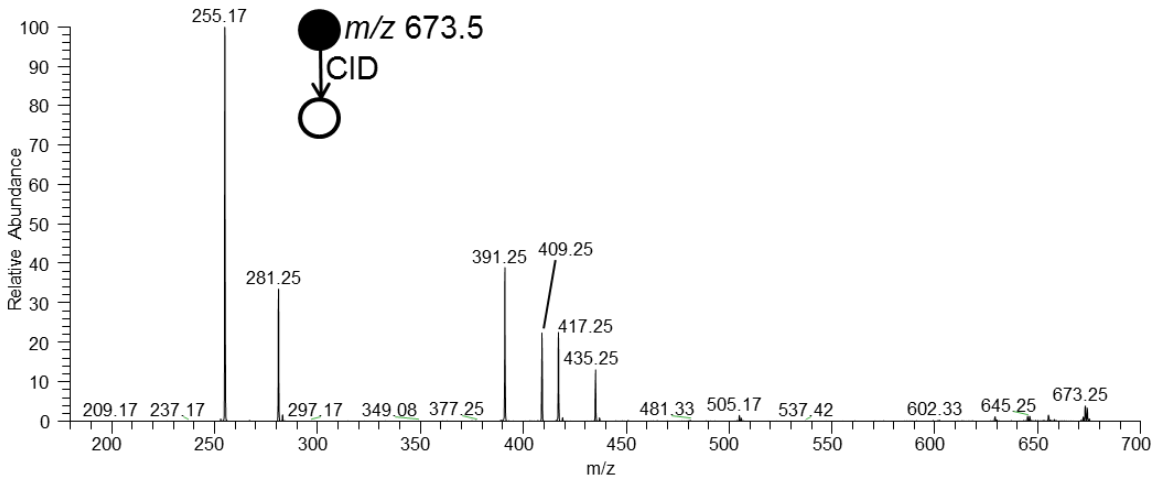

Fig. S13. Low-energy CID MS/MS spectrum of the ions at *m/z* 673.5 detected from rat brain tissue in negative ion mode using the linear ion trap. Fragment ions supporting the assignment of $[PA(16:0\_18:1)\text{-}H]^-$ are found at *m/*z 391 and 409 (loss of 18:1 fatty acid and ketene), *m/*z 417 and 435 (loss of 16:0 as fatty acid and ketene), *m/*z 281 (18:1 fatty acid) and *m/*z 255 (16:0 fatty acid). Due to the isolation width of 1 *m/z* unit additional isobaric and isomeric lipids are also fragmented giving rise to additional fragment ions.

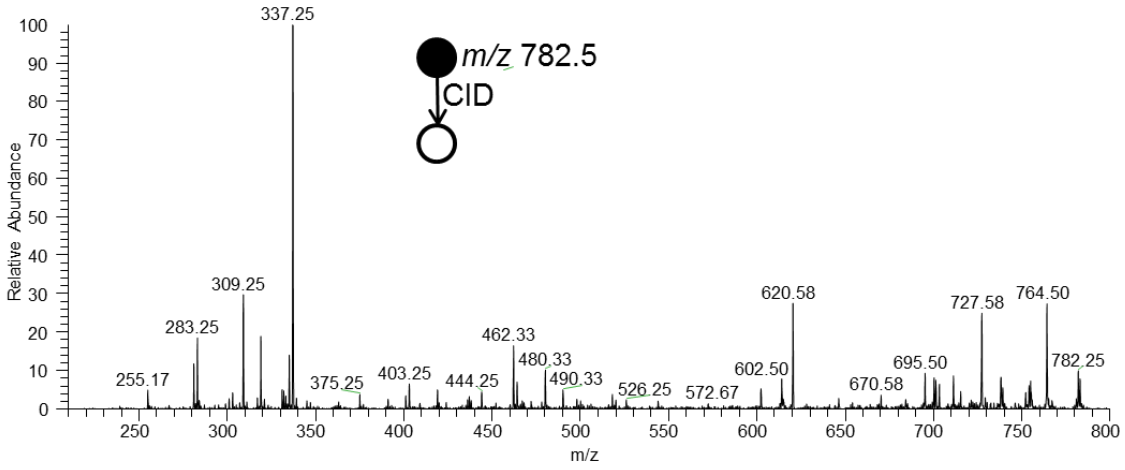

Fig. S14. Low-energy CID MS/MS spectrum of the ions at *m/z* 782.5 detected from rat brain tissue in negative ion mode using the linear ion trap. Fragment ions supporting the assignment of $[GalCer(d40:1)\text{-}H]^-$ are found at *m/*z 602 and 620 (loss of glucose and [glucose-H_2O]). Due to the isolation width of 1 *m/z* unit additional isobaric and isomeric lipids are also fragmented giving rise to additional fragment ions.

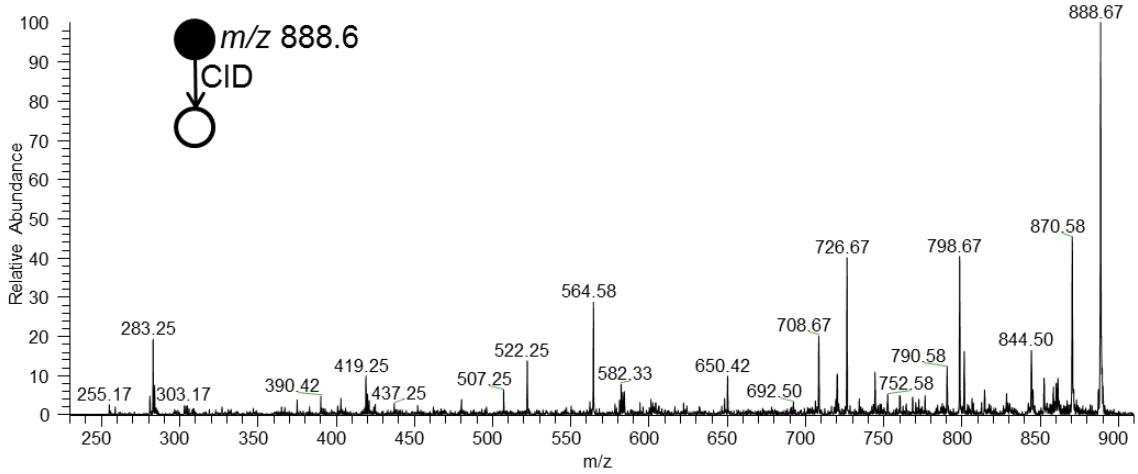

Fig. S15. Low-energy CID MS/MS spectrum of the ions at *m/z* 888.6 detected from rat brain tissue in negative ion mode using the linear ion trap. Fragment ions supporting the assignment of $[ST(d18:1/24:1)]^-$ are found at *m/z* 522 (consecutive loss of 24:1 fatty acyl and water), *m/z* 390 and 650 (both related to loss of d18:1 long chain base as $HCOCH{=}CH(CH_2)_{12}CH_3$) as described in reference[4]). Due to the isolation width of 1 *m/z* unit additional isobaric and isomeric lipids are also fragmented giving rise to additional fragment ions.

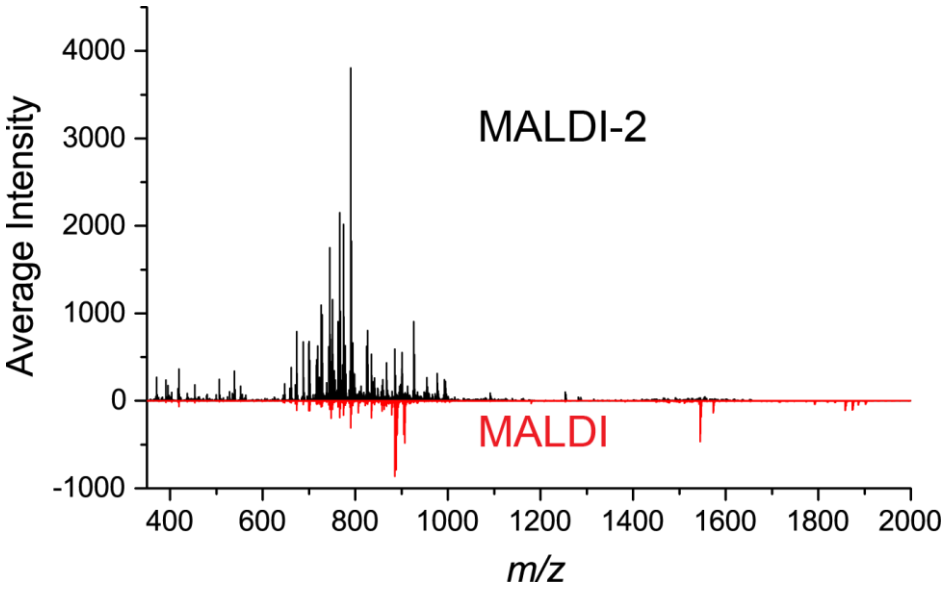

Fig. S16. Full average negative ion MALDI-2 (top) and conventional MALDI (bottom) mass spectra acquired from a rat brain tissue section and showing the *m/z* range of 350-2000. The same data set as for Fig. 4a of the main text was evaluated.

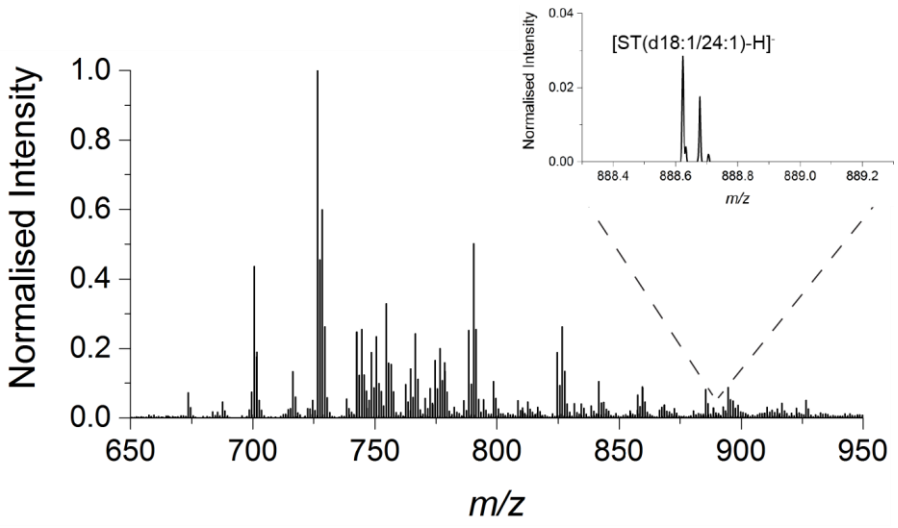

Fig. S17. Negative ion MALDI-2 mass spectrum from norharmane-coated rat brain using a MALDI-2 laser pulse energy of 50 µJ at 280 nm (instead of 800 µJ used to record all other presented MALDI-2 data). Even at this low energy a significant reduction is the ST(d18:1/24:1)-H]$^-$ signal is observed upon MALDI-2.

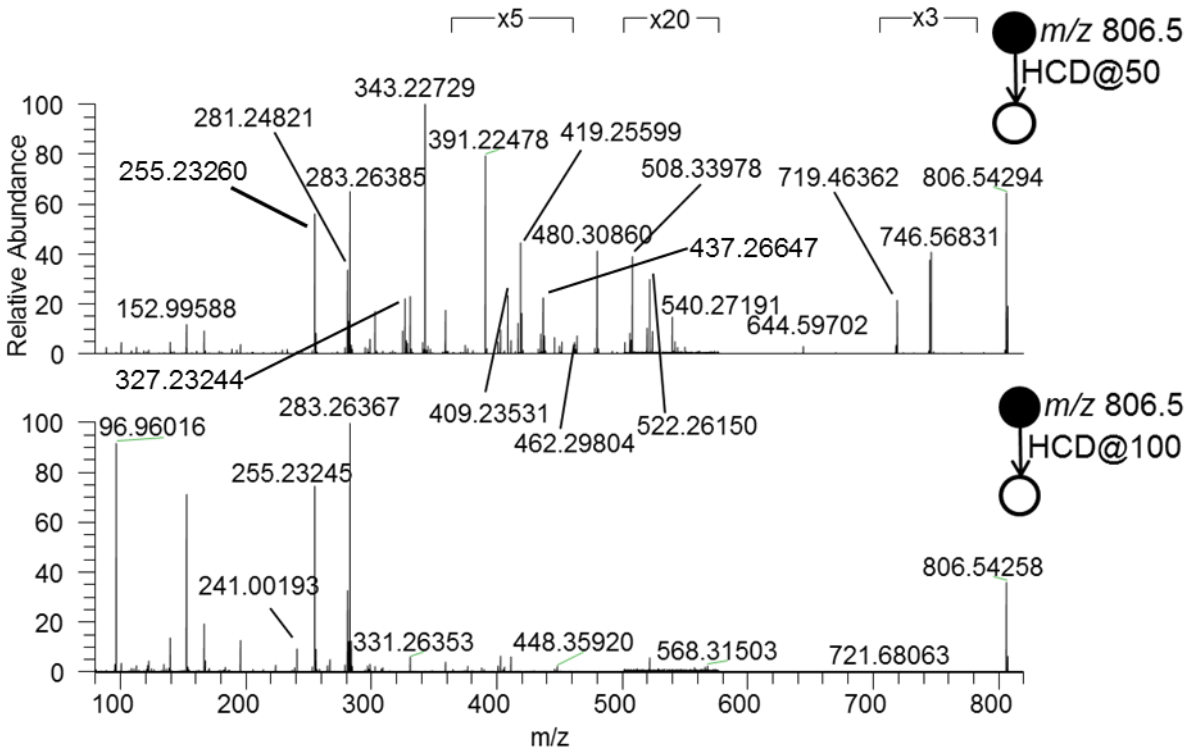

Fig. S18. Negative ion mode higher energy collisional dissociation (HCD) MS/MS spectrum of the isobaric ion series found in the *m/z* window between *m/z* 806.47-806.60 as shown in Fig. 5. Fragment ions were detected with the Orbitrap (mass resolution setting 240,000 FWHM). The ions found at *m/z* 806.5 in the rat brain tissue were fragmented with normalised collision energies of 50 (top) and 100 (bottom). Fragment ion(s) supporting the assignment of $[PS(16:0\_22:6)-H]^-$ are found at *m/z* 719.46362 (loss of serine-H_2O, -2.9 ppm), *m/z* 391.22478 and 409.23531 (loss of [serine-H_2O] followed by loss of 22:6 as fatty acid, -1.8 ppm, and ketene, -1.8 ppm), *m/z* 463.22457 (loss of [serine-H_2O] followed by loss of 16:0 as fatty acid, -2.0 ppm, *m/z* 327.23244 (22:6 fatty acid, -1.6 ppm) and *m/z* 255.23263 (16:0 fatty acid, -1.3 ppm) Fragments supporting the assignment of $[PE(40:6)(OH)-H]^-$ are found at *m/z* 462.29804 and 480.30860 (loss of 22:6(OH) fatty acid, -2.1 ppm, and ketene, -2.0 ppm), *m/z* 522.26150 and 540.27191 (loss of 18:0 fatty acid, -2.1 ppm, and ketene, -2.3 ppm), *m/z* 343.22729 (22:6(OH) fatty acid, -1.6 ppm) and *m/z* 283.26385 (18:0 fatty acid, -1.4 ppm). Fragment ions supporting the assignment of $[PC(34:0)+HCO_2]^-$ are found at *m/z* 746.56831 (loss of methyl formate, -2.9 ppm), *m/z* 462.29804 and 480.30860 (loss of 18:0 as fatty acid, -2.3 ppm, and ketene, -2.2 ppm, from the $[PC(34:0)-CH_3-H]^-$ ion), *m/z* 508.33978 (loss of 16:0 ketene, -2.1 ppm, from the $[PC(34:0)-CH_3-H]^-$ ion), *m/z* 255.23260 (16:0 fatty acid, -1.8 ppm) and *m/z* 283.26385 (18:0 fatty acid, -1.4 ppm). Fragments supporting the assignment of $[ST(d36:1)-H]^-$ are found at *m/z* 96.96016 (HSO_4^-, 0.5 ppm) and *m/z* 241.00193 ([galactose 3-sulfate-H_2O]$^-$, -1.8 ppm). Unambiguous fragments for $[PE(P-42:4)-H]^-$/$[PE(O-42:5-H]^-$ (*i.e.*, neutral loss of the esterified fatty acid) were either absent or present at very low abundance. Due to the isolation width 1 of *m/z* unit additional isobaric and isomeric lipids are also fragmented giving rise to additional fragment ions.

References

1. G. B. Eijkel, B. Kükrer Kaletaş, I. M. van der Wiel, J. M. Kros, T. M. Luider and R. M. A. Heeren, *Surf. Interface Anal.*, 2009, **41**, 675-685.
2. G. Liebisch, J. A. Vizcaíno, H. Köfeler, M. Trötzmüller, W. J. Griffiths, G. Schmitz, F. Spener and M. J. O. Wakelam, *J. Lipid Res.*, 2013, **54**, 1523-1530.
3. E. Fahy, S. Subramaniam, H. A. Brown, C. K. Glass, A. H. Merrill, Jr., R. C. Murphy, C. R. H. Raetz, D. W. Russell, Y. Seyama, W. Shaw, T. Shimizu, F. Spener, G. van Meer, M. S. VanNieuwenhze, S. H. White, J. L. Witztum and E. A. Dennis, *J. Lipid Res.*, 2005, **46**, 839-862.
4. F.-F. Hsu and J. Turk, *J. Am. Soc. Mass. Spectrom.*, 2004, **15**, 536-546.